Ocean tide loading - where we are standing

H.-G Scherneck, M.S. Bos and R.M.S Fernandes

20 July 2017

Introduction

Ocean tides cause up to centimetre level displacements of the Earth surface that are observed by space geodetic techniques. Therefore, ocean tide loading corrections have been in use in VLBI software for over thirty years. The GNSS technique is more recent but the number of stations has grown rapidly to a few thousands and the IGS is striving for comparable accuracy demands as the IVS. Anticipating the foreseeable work load of computing ocean tide loading coefficients, Scherneck and Bos (2002) launched an automated, internet-based user service in 2001, called the Free Ocean Tide Loading Provider (henceforth called OLP). An OLP client may choose among 27 ocean tide models and specify up to 100 station positions per request. The computation of coefficients is based on a convolution integral of a global tide model with a Green's function. The latter represents the deformation of the Earth's surface due to a point load on an elastic, spherically symmetric Earth (Farrell 1972; Bos and Scherneck 2013). In the next sections we present the details of the computation of the OTL coefficients and discuss the improvements of the OLP we envision for the near future.

Ocean tide Models and Coastlines

Since the launch of the TOPEX/Poseidon satellite in 1992, the oceanographic community has produced global ocean tide models with ever increasing spatial resolution, from a wider range of observation sources, and has extended the park of methods in charting and hydrodynamic modelling. Table 1 gives a short overview of the ocean tide models that have been published over the years. For historic reasons we also include the model of Schwiderski (1980), which predates the satellite altimetry era, that has a spatial resolution of 1°. The most recent ocean tide models provided by Toulouse group, FES2012 and FES2014b, has a grid spacing of 1/16°. More details about the early ocean tide models are given by Shum et al. (1997) while Stammer et al. (2014) review the more recent ones.

Table 1: Time line of ocean tide models, time they became available, number of nodes per degree (reciprocal grid constant) and the number of frequencies (waves). The last column contains the thickness of the tide layer for harmonic M_2 that needs to be added to each model to conserve the tidal water mass.

Model	year	1/resol	nr. of waves	thickness (mm)
Schwiderski	1980	1	11	7.30
TPXO.5	1994	2	11	0.90
CSR3	1994	2	8	0.41
CSR4	1994	2	8	0.56
FES94.1	1994	2	11	3.80
FES95.2	1995	2	12	1.19
FES98	1998	4	11	1.74
FES99	1999	4	15	1.33
GOT99.2b	1999	2	11	0.22
NAO.99b	2000	2	23	1.32
GOT00.2	2000	2	11	0.15
FES2004	2004	8	17	0.57
TPXO.6.2	2004	4	11	0.54
AG06	2006	4	11	0.26
TPXO.7.0	2002	4	11	0.23
TPXO.7.1	2007	4	11	0.22
EOT08a	2008	8	13	0.46
TPXO.7.2	2009	4	11	0.06
DTU10	2010	8	13	0.47
EOT11a	2011	8	14	0.61
GOT4.7/GOT4.8	2011	2	12	0.10
OSU12	2012	4	13	0.30
FES2012	2012	16	11	0.49
Hamtide	2014	8	11	0.11
TPXO8-Atlas	2014	30	9	0.21
FES2014b	2014	16	34	0.16

Figure 1 shows for harmonic M_2 the vector difference between Schwiderski-FES94.1, FES2004-GOT00.2 and between FES2014-TPXO.8. The first shows difference of the order of 10 cm, indicating the tremendous effect of including satellite altimetry data into the model. The second panel shows that around 2000-2004 there were still remaining errors near the coast and in the polar region. The third panel shows that with the most recent models these errors are further reduced.

The models with 1/8° spatial resolution already required a wall clock computing time of up to two hours per OLP request with hundred stations. On an average day, the OLP machine at Onsala is occupied with jobs for more than 12 hours.

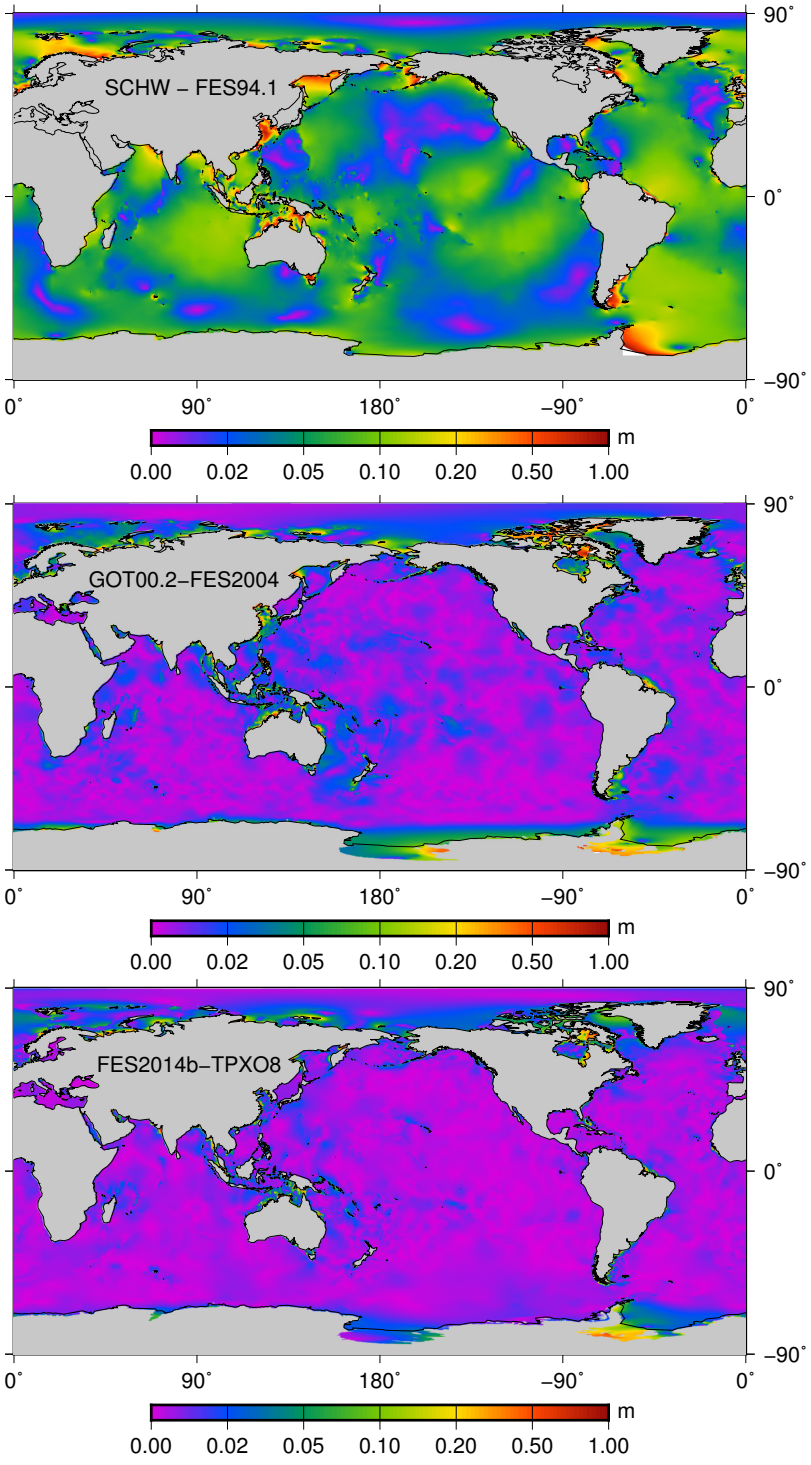

Figure 1: The difference between OTL computed using Schwiderski & FES94.1 (top), FES2004 & GOT00.2 (middle) and FES2014b & TPXO.8 (bottom), all for M_2 vertical component

The recent models would raise this four-fold, creating an ever-increasing backlog of OTL requests.

As a provisory solution, requests involving FES2012 or FES2014b are currently relayed to SEGAL. There, the computation uses reduced ocean grids at 1/4° in the open ocean and the 1/16° resolution near the coast in order to represent the complex shelf and bay tides. The latter also ensures a better fit with the coastline. Penna et al. (2008) showed that the coastline resolution is a critical step; especially with the early models that have grid constants of one or one-half degree, tide loads on complicated coasts are insufficiently represented when geodetic sites are located there at short distances. The OLP employs a quad-tree algorithm that inter- and extrapolates at ever finer resolution between the global grid and the coastline, which is take from the high-resolution database of the GMT package (Bos and Baker 2005).

The higher resolution of the recent models implies a slightly lower accuracy demand on the quad-tree filling between regular grid and coastline. Yet, this step does not appear to become obsolete if we require sub-millimetre precision for the leading tide M_2 (as a rule of thumb, the error level is about two times the M_2 error when all eleven tide waves are included; this estimate takes also the missing signal from unrepresented waves into account). As an example of an outright error in ocean representation of the global FES2014b grid is shown in Figure 2. It represents the area of the southern Malacca peninsula and one can note the white area in the left diagram. Fortunately, the tide is low there and the nearest GNSS station of the IGS station, NTUS, is at a respectable distance (marked with a black cross). Also note that much fewer wet nodes are located on land than dry ones in the sea, judging from the GMT full-resolution coastline. Recently a version of FES2014b has been made available that has tidal grid cells extrapolated over land, resolving this problem. However, such an extrapolation is also performed inside our OTL software. The OTL map to the right is computed using the fast gridding method, see section 3.

Ocean tide models do not always conserve water mass during a tidal cycle. To solve this problem, a thin tide layer with a certain phase-lag is normally added to the model. The thickness of this layer for harmonic M_2 is given in the last column of Table 1 which shows that this problem was larger for the older models. For FES94.1 (again M_2), including mass conservation can change the OTL amplitude by 0.2 mm while for FES2012 this value is less than 0.03mm.

Fast OTL computations and Green's functions

In response to the afore mentioned long computation times, a fast Fourier algorithm was devised to compute the loading effects from the global, regular tide grids. It computes the global deformation field with the same grid constants. Thus, the results can be stored once-for-all. Assuming the OTL map has the

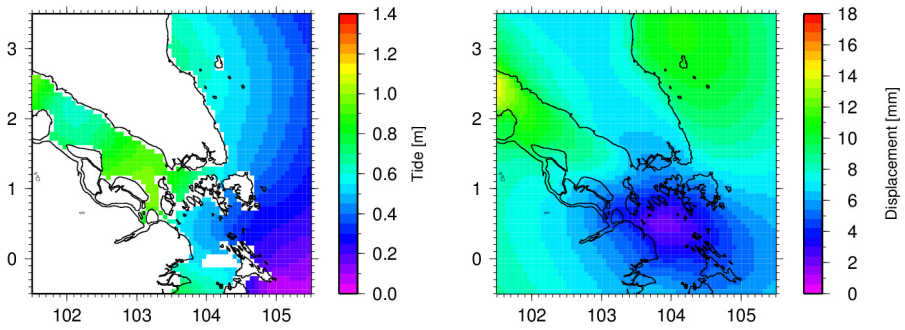

Figure 2: The left panel shows the land-sea representation error in FES2014b at the southern Malacca peninsula, note the white area in the left diagram. Fortunately, the tide is low there and the nearest GNSS station of the IGS station, NTUS, is at a respectable distance (marked with an X). The right panel shows the corresponding OTL displacement (M_2, up component).

same grid resolution as that of the ocean tide model, the CPU-time is proportional to $N^3 \log N$, where N is the number of grid nodes in one dimension. For the traditional convolution integral approach, this would be N^4. The whole set of global OTL maps can be computed in 25 hours (next generation ocean tide models would eventually need a more powerful computer) instead of months using a program such as CARGA (Bos and Baker 2005). The new implementation of the Fast OTL algorithm strikes a balance between speed and precision; for instance, the Green's functions hemispheric symmetry is utilised, and the function is integrated over grid boxes if they are within a critical distance.

For some stations that are within a 10-50 km range of the coast, we noted that it is still necessary to subdivide the ocean tide grid cells around the station to keep the numerical error below the 0.1-0.3 mm level per harmonic. However, this quad-tree subdivision is only necessary in a limited region near these sites. Efforts to come to specific thresholds and terms with this task are currently in progress. The ambition is that differences between different ocean models would stand out above measures of increased precision, where the latter should arrive at less than a millimetre when time series are produced, i.e. all waves are added together. Figure 3 shows an example for the spread of loading phasors from a sample of ocean tide models, Green's functions and processing methods for VLBI station BRFT, Fortaleza, Brazil, harmonic M_2, up component. It shows OTL values computed using the internet ocean tide loading provider with high-resolution coastlines (olp) and the fast mapping algorithm (map), with no coastline refinement. It also shows OTL values computed using various Green's functions such as the one of Gutenberg-Bullen (GB), Anderson and Dziewonski (PREM). The latter has been computed assuming a pure elastic Earth (real) or a constant absorption band from 1s to the period of M_2 (cmplx). The latter includes anelasticity effects that are mostly produced in the asthenosphere, see

Bos et al. (2015) for more details.

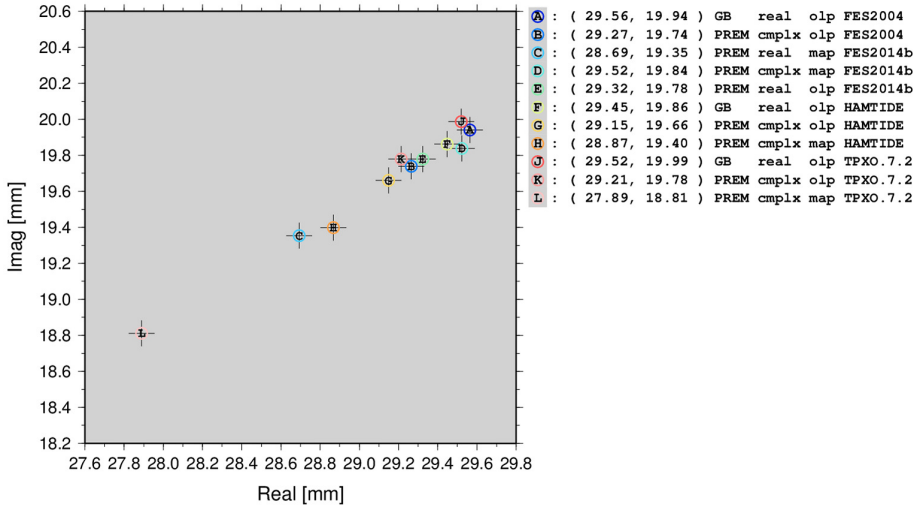

Figure 3: Loading phasors for vertical displacement of tide M2 at the VLBI site BRFT, Fortaleza, Brazil. Shorthands for Green's functions: Earth structure from GB - Gutenberg-Bullen, PREM - Anderson and Dziewonski; real - elastic earth, cmplx - anelastic earth

The reader might wonder why do we keep the tide waves of the OLP to the set published by Schwiderski (1980)? First, although recent catalogues include species in addition to S_{sa}, M_m, M_f, Q_1, O_1, P_1, K_1, N_2, M_2, S_2 and K_2, the sets are inconsistent and thus cumbersome to employ in routine geodetic analyses. Second, the BLQ format adopted in a range of softwares still seems to enjoy wide use. If an option to include all available waves pertaining to a model catalogue is introduced, the tables of loading coefficients would be issued in the HARPOS format thanks to its extendibility. Readers may notify us of their opinion.

OTL time series

In the previous section, we noted that the OTL coefficients are given as a set of amplitudes and phase-lags for 11 major harmonics. The displacement time series are computed by simply summing the various periodic functions:

$$u(t) = \sum_{i=1}^{11} A_i \sin(\omega_i t + \phi_i)$$

where A_i is the amplitude and ϕ the phase-lag value provided by the OLP.

However, the full tidal potential has many more as shown in Figure. 4, see also Wenzel (1997) or Agnew (2007). These must be considered if one produces an accurate time series from the OTL coefficients.

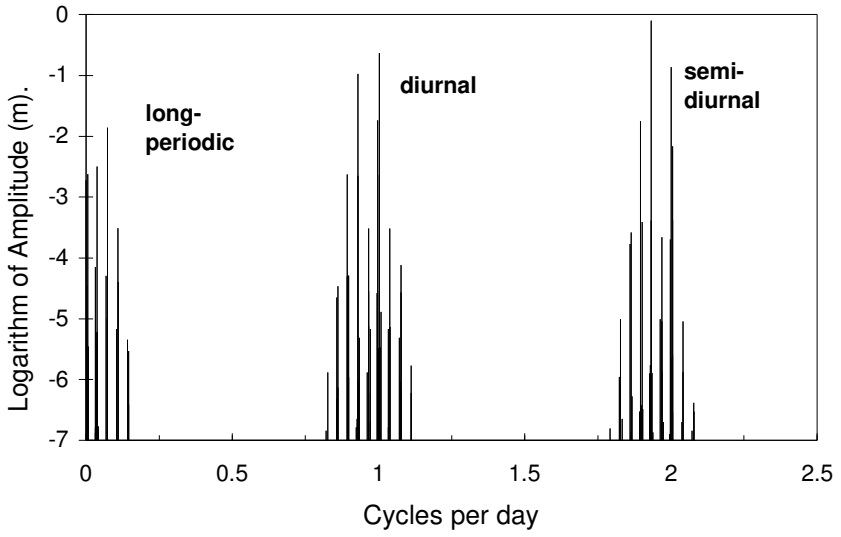

Figure 4: Amplitude of the harmonics listed in the Tamura tidal potential

To include the effect of the other harmonics, several methods are in use. The simplest one is to apply nodal corrections (Chap 7, McCarthy and Petit 2003) which was the IERS convention up to 2010. Another approach is to assume that the dynamic response of the ocean to the forcing of the of the tidal potential is similar for a range of frequencies. This is called tidal admittance and was advocated by Munk and Cartwright (1966). As a result, the fraction of OTL displacement divided by the amplitude of the tidal potential will also be a smooth function over this frequency range. Agnew has implemented this approach in his `hardisp` program which is now part of the IERS conventions (Chap 7, Petit and Luzum (2010)). It fits a spline through the 4 admittance values in the diurnal and semi-diurnal group respectively. A set of straight lines is fitted to the 3 long period tides.

In the previous section we already noted that the BLQ file might in the future include more harmonics and here we tested the effect of including harmonics: J_1, S_1, $2N2$, μ_2, L_2, R_2 and T_2. We included these harmonics into `hardisp` and computed the associated OTL values for BRFT, vertical component, using FES2014b. The resulting admittance functions are shown for the in-phase and out-phase parts in Figure 6.

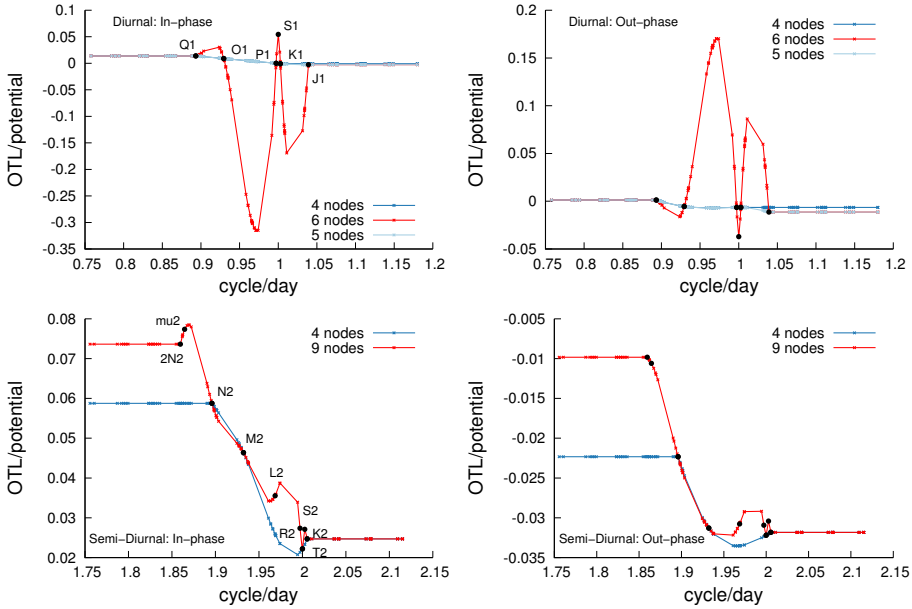

Figure 5: Admittance of the OTL at BRFT for the diurnal and semi-diurnal group, for the in-phase and out-phase parts. Note the influence of S_1 in the diurnal group.

This figure shows the large influence of S_1 on the admittance function. S_1 is not only created by the gravitational attraction of the Sun but also by the heat of the Sun. It is therefore called a radiational wave and it distorts the smooth admittance function. If S_1 is included, then for BRFT, vertical component, the difference between the predicted time series has a standard deviation of 3.7 mm (maximum of 8 mm). When S_1 is omitted, this reduces to a standard deviation of 0.4 mm (maximum 1.2 mm). The latter values is smaller but can still be detected by space geodetic technique and therefore this topic requires further investigation.

The harmonic with the lowest frequency is S_{sa} with a period of half a year. However, using tidal admittance, also the OTL at the 18.6 year period is included in the `hardisp` program. Its effect is largest near the poles and equator. For the stations at Ny-Alesund (NYAL) and Forteleza (BRFT), the OTL due to ocean tides with a period longer than 100 days is shown in Figure 5. It demonstrates that both the 18.6 year and S_{ssa} harmonics can influence the position up to the mm level and therefore should be included in the analysis. A curious fact is that the 18.6 year OTL deformation is computed using elastic properties of the Earth that are valid at 1s. If these elastic properties are constant over 8 decades of frequency remains to be validated.

Outlook

18.6 year OTL tide

Green's functions

References

Agnew D (2007) Earth Tides. In: Herring T (ed) Treatise on geophysics: Geodesy. pp 163–195

Bos MS, Baker TF (2005) An estimation of the errors in the gravity ocean tide loading computations. J Geodesy 79:50–63.

Bos MS, Penna NT, Clarke PJ, T. F. Baker (2015) Ocean tide loading displacements in western Europe. Part 2: GPS-observed anelastic dispersion in the asthenosphere. Journal of Geophysical Research 120:online. doi: 10.1002/2015JB011884

Bos MS, Scherneck H-G (2013) Computation of green's functions for ocean tide loading. In: Xu G (ed) Sciences of geodesy - ii. Springer Berlin Heidelberg, pp 1–52

Farrell WE (1972) Deformation of the Earth by Surface Loads. Rev Geophys

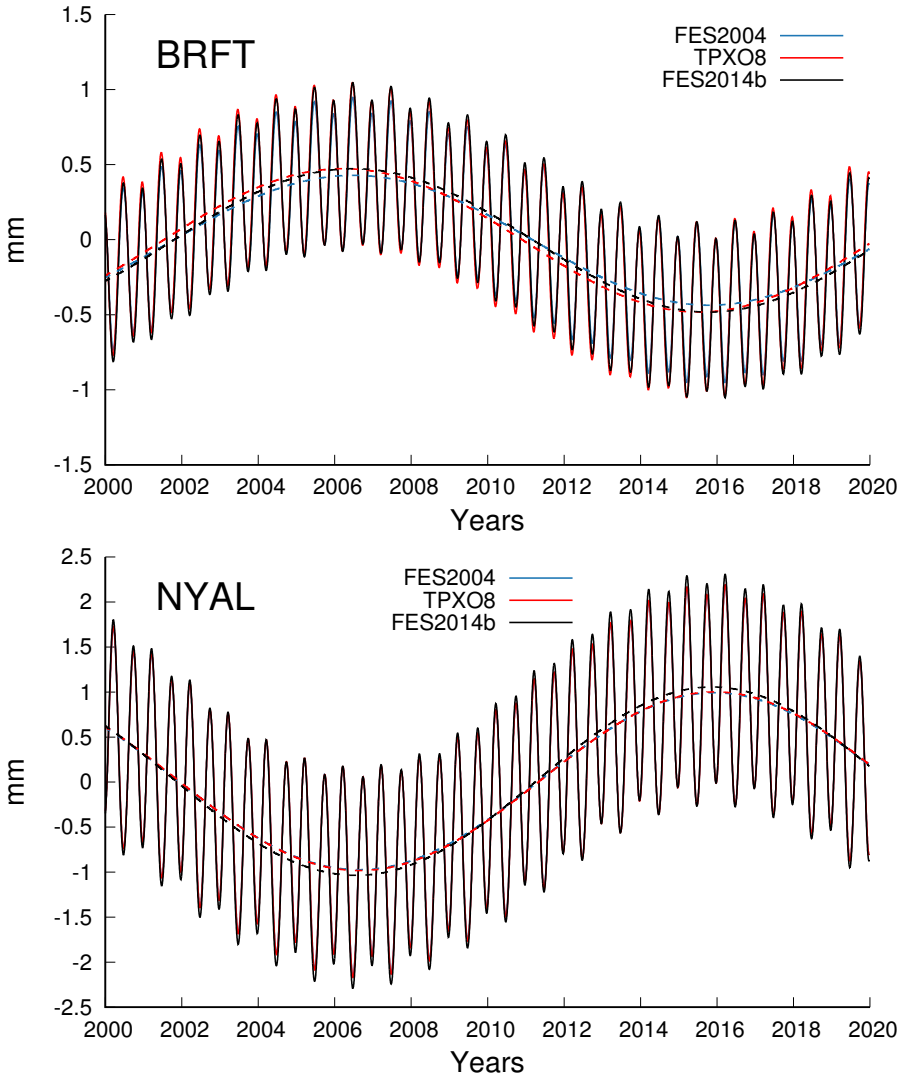

Figure 6: vertical OTL due to ocean tides with a period longer than 100 days at Ny-Alesund and Forteleza. The dotted lines show the 18.6 year OTL contribution

Space Phys 10:761–797.

McCarthy DD, Petit G (eds) (2003) IERS technical note 32. Frankfurt am Main: Verlag des Bundesamts für Kartographie und Geodäsie, ISBN 3-89888-884-3

Munk WH, Cartwright DE (1966) Tidal spectroscopy and prediction. Phil Trans Roy Soc London, Ser A 259:533–581.

Penna NT, Bos MS, Baker TF, Scherneck H (2008) Assessing the accuracy of predicted ocean tide loading displacement values. Journal of Geodesy 82:893–907. doi: 10.1007/s00190-008-0220-2

Petit G, Luzum B (eds) (2010) IERS technical note 36. Frankfurt am Main: Verlag des Bundesamts für Kartographie und Geodäsie, ISBN 3-89888-989-6

Scherneck H-G, Bos MS (2002) Displacements due to ocean tide and atmospheric loading using modern sea level records. In: Vandenberg NR, Baver KD (eds) International vlbi service for geodesy and astrometry 2002 general meeting proceedings.

Schwiderski EW (1980) On charting global ocean tides. Rev Geophys Space Phys 18:243–268.

Shum CK, Woodworth PL, Andersen OB, Egbert GD, Francis O, King C, Klosko SM, Le Provost C, Li X, Molines JM, Parke ME, Ray RD, Schlax ML, Stammer D, Tierney CC, Vincent P, Wunch CI (1997) Accuracy assesment of recent ocean tide models. J Geophys Res 102:25, 173–25, 194.

Stammer D, Ray RD, Andersen OB, Arbic BK, Bosch W, Carrère L, Cheng Y, Chinn DS, Dushaw BD, Egbert GD, Erofeeva SY, Fok HS, Green JAM, Griffiths S, King MA, Lapin V, Lemoine FG, Luthcke SB, Lyard F, Morison J, Müller M, Padman L, Richman JG, Shriver JF, Shum CK, Taguchi E, Yi Y (2014) Accuracy assessment of global barotropic ocean tide models. Reviews of Geophysics 52:243–282. doi: 10.1002/2014RG000450

Wenzel H-G (1997) Tide-generating potential for the earth. In: Wilhelm H, Zürn W, Wenzel H-G (eds) Tidal phenomena. Springer,